Journal of Nuclear Materials 390–391 (2009) 1145–1148

Contents lists available at ScienceDirect

Journal of Nuclear Materials

journal homepage: www.elsevier.com/locate/jnucmat

Design status of ITER visible/IR outer strike point view

C.J. Lasnier *, L.G. Seppala, K. Morris, M.E. Fenstermacher, M. Groth

Lawrence Livermore National Laboratory, Livermore, CA 94550, USA

ARTICLE INFO

PACS:
52.55
52.70
52.25.R
87.58.W

ABSTRACT

For ITER visible/IR imaging of the outer strike point from the six upper ports currently assigned, we show an optical design that provides a 4 mm Airy disk at 5 μm wavelength at the farthest point in the field of view (much smaller in the visible), with as complete toroidal coverage of the vertical target as possible. Plasma and optical effects provide fundamental limits on the performance and design of the system. Some effects involve interactions of the surfaces with the plasma, such as plasma transport and deposition of material on the surfaces to be viewed, plasma damage to those surfaces, and molecular emission by the plasma at IR wavelengths. We discuss a detailed optical design including the endoscope concept, entrance aperture and collection head, relay optics, and camera specifications and performance. We assess integration times for capture of IR emission from surfaces and visible line emission predicted by boundary modeling.

1. Introduction

IR and visible camera views of the ITER divertor outer strike point (OSP) from six upper ports are included in the baseline diagnostic set. The IR system is to monitor surface temperatures, and the visible is to monitor hydrogenic and impurity emission from the divertor. The goal is to provide maximum toroidal coverage of the outer divertor plate, for protection of the divertor and for physics measurements. Due to the geometry, 90% of the outer divertor plate surface is accessible. Parts of this area are seen near grazing incidence, where a useful IR measurement is not feasible. We show an endoscope design [1] compatible with an upper port, which provides a 4 mm Airy disk at 5 μm wavelength at the farthest point in the field of view, with better resolution in the visible. Numerous effects limit the performance or design of the system, including diffraction, uncertainty in emissivity, reflections, deposition, erosion and cracking on surfaces, molecular and bremsstraliung emission in plasma, heating of optics by conduction, and by thermal and nuclear radiation, damage to transmissive optics by neutron bombardment, and damage to first mirrors by neutral particle bombardment.

The IR system was specified by the ITER organization to measure temperatures from 200 to 2500 °C, (now increased to 200–3600 °C) with time resolution of 20 ms for temperatures above 1000 °C (2 ms below 1000 °C) and spatial resolution of 3 mm. The visible system requirement was 100 ms time resolution. We note that the optical system design described here has a spatial resolution of 4 mm, not the specified 3 mm. This is due to allowed sizes of the optics in the port tube, which constrain the size of the entrance aperture. Further information on the design is available in detailed technical reports [2,3].

2. The optical design

The concept for the diagnostic is an insertable endoscope contained in a tube, similar to the system built for JET by the CEA [4]. The ITER system described here has the entrance aperture and first mirrors in vacuum, while the JET optics are outside the primary vacuum in an evacuated re-entrant tube. An overview of the optical system is shown in Fig. 1. A small entrance aperture reduces damage to the first mirror by plasma and neutral particles. The central part of the light beam is picked off inside the vacuum windows by a 45° angled mirror to be used by the visible system. The visible light is sent through its own set of vacuum windows. Next the visible and IR beam are each relayed across the port interspace (in air) by a separate lens relay, each optimized for appropriate wavelengths. This is followed by matching optics that focus the image onto a camera.

A small entrance aperture would protect the first mirror, but a large one would minimize diffraction. The maximum size of the aperture is limited by the size of the aperture image that can be relayed through the port tube, set by the diameter of the optics that fit and the spacing between optics. A closer spacing of optics allows a larger entrance aperture, but the spacing is constrained by the vulnerability of transmissive optics to neutron damage inside the port tube. The present design uses a 21 mm entrance aperture.

* Corresponding author. Address: Lawrence Livermore National Laboratory, 13-363, General Atomics, P.O. Box 85608, San Diego, CA 92186-5608, USA.
E-mail address: Lasnier@llnl.gov (C.J. Lasnier).

0022-3115/$ - see front matter © 2009 Elsevier B.V. All rights reserved.
doi:10.1016/j.jnucmat.2009.01.273

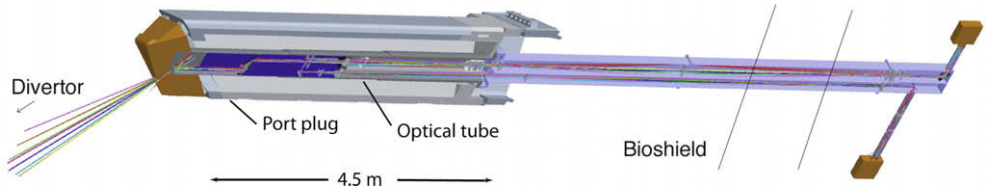

Fig. 1. Cutaway of optical path, showing ray tracing. The optical tube passes through the port plug and views through an aperture in the Blanket Shield Module. For compactness the drawing has been rotated clockwise 12.5°. The cameras are located outside the bioshield.

The collection head consists of the entrance aperture, first mirror, and second mirror (see Fig. 2). The first mirror is a curved aspheric focusing mirror, which sends the light to the second, a plane mirror whose purpose is to redirect the light down the tube. The entrance aperture is a hole in this secondary mirror and produces a small blind spot that is positioned in a non-critical part of the image. Dogleg mirrors following the collector head block direct neutron radiation, and neutron shielding surrounds the beam path.

Due to the darkening of lenses under neutron bombardment, this design minimizes visible-light lenses in the vacuum portion of the port tube, with only one CaF_2/silica doublet just inside the vacuum window, where the neutron radiation is lowest due to neutron shielding installed in the port tube. Damage by 14 Mev neutrons to CaF_2, ZnSe, and the other optical materials must be tested before the final design is chosen and constructed.

IR lenses are also problematic in the port tube due high temperatures. Hot IR lenses emit spurious infrared light, and for germanium the focal length is temperature-dependent. A Cassegrain telescope with an aspheric ZnSe corrector plate collects the IR light. Light obstructed by the secondary mirror of the IR Cassegrain is sent to the visible camera by two flat mirrors (Fig. 3). The ZnSe corrector plate will be relatively safe from neutron damage near the outer end of the port tube.

Double vacuum windows (94 mm aperture) are used for tritium safety. We use silica for the visible-light windows, and sapphire for the IR. Putting the Cassegrain inside the vacuum allows smaller IR windows, since the focused beam is smaller. Outside the vacuum, the lens relays in the port interspace consist of groups of lenses of materials appropriate to the wavelength. The IR lens materials are ZnSe, ZnS and Ge. The visible lenses are of CaF_2 and silica. The light is relayed through the bioshield, which is a thick neutron-shielding wall outside the port interspace.

Lens sets are used to focus the image onto the camera detectors, and turning mirrors allow the camera to be positioned out of the direct path of residual neutrons passing through the opening in the bioshield. The visible camera-matching section contains lenses of CaF_2, silica and LF5G15, a radiation-resistant glass available from Schott AG. IR lenses are again ZnSe, ZnS and Ge.

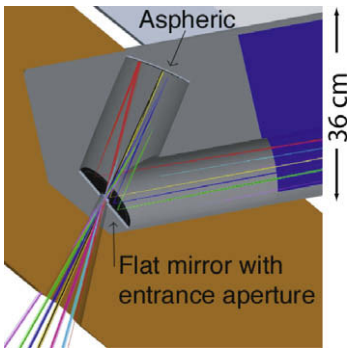

Fig. 2. Side view of the optical head. The viewing aperture is located within the Blanket Shield Module for the port (the shaded area surrounding the mirrors).

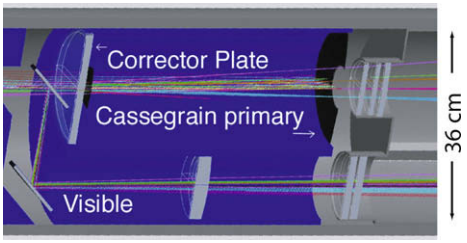

Fig. 3. Side view of optics in the outer part of the port plug. The dark shaded volumes represent neutron shielding, which surrounds the optics and beam path. The visible light shunt, IR Cassegrain, and vacuum windows are shown.

In order to produce the 4 mm spatial resolution over the desired field of view, the camera detectors must be 3500 pixels wide. The IR detector is 70 mm wide, with 0.02 mm pixels. The visible detector is 35 mm, with 0.01 mm pixels. This gives pixel sizes of 1.5 mm at the most distant part of the vertical target. At the near edge of the field of view the target is viewed at a steeper angle to the surface and the spatial resolution is reduced compared to nearby horizontal surfaces.

IR cameras are commercially available with pixel sizes near 0.02 mm, but not the pixel count or 50 kHz frame rate required, so further development is required. Visible cameras have the required pixel size and pixel count, but frame rates of only 3–5 Hz compared to the required 10 Hz. In fact a much higher frame rate is desirable for analyzing transient behavior such as ELMs and disruptions. (We expect that the speed of commercially available visible-light cameras will continue to improve rapidly.) The available emitted light from impurities, which will determine the integration time needed for desired signal-to-noise ratios, will fix the ultimate frame rate limit for visible cameras.

A calibration system is not yet designed. We anticipate that the full system must be calibrated before installation, and a shutter with a temperature-controlled emitting surface on the back will be needed to maintain the IR calibration. A concept still must be developed for maintaining calibration of the visible system and monitoring changes in optical throughput.

3. Limitations on the design and performance

3.1. Optical effects

The IR view is diffraction-limited by the 21 mm entrance aperture, with an object distance up to 11.5 m. The modulation transfer function (MTF) for the IR is shown in Fig. 4. The MTF shows the contrast as a function of spatial frequency. Using only the center part of the full beam reduces the effective aperture of the visible optics. However, the visible system spatial resolution is still superior to the IR because the shorter wavelengths diffract less.

To obtain the surface temperature from a single spectral measurement, the emissivity of the surface must be known, which for new carbon approaches 0.9. That of a metal surface can be 0.1 or less, and depends in detail on the surface preparation, with

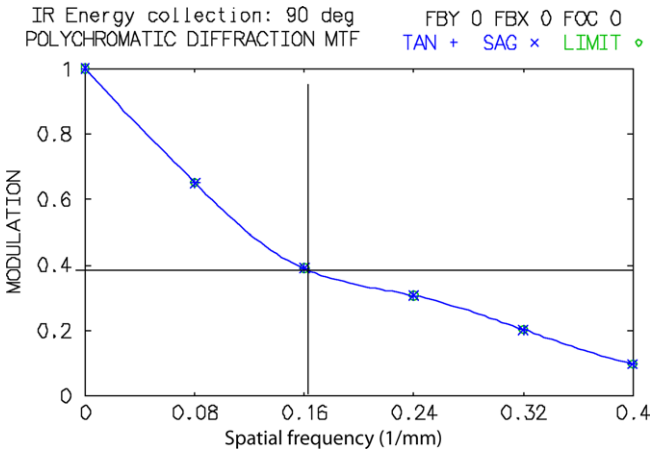

Fig. 4. Modulation transfer function (MTF), showing the contrast at various spatial frequencies.

a polished surface being lowest. At the opposite extreme, a knurled surface provides tiny emission cavities that raise the emissivity. As the roughness of a metal surface changes due to plasma interaction, the emissivity will change. Emissivity values recorded in the literature for tungsten [5] vary from 0.05 to 0.5. Two-color or multi-color measurements sample the thermal emission at two or more wavelengths and a blackbody spectrum is fitted to the results [6,7]. In this case, only relative emission intensities are needed to get the surface temperature. However, for hot-spots less than the size of a pixel due to tile joints or dust, the absolutely calibrated emission is useful in addition to the two-color analysis [8].

If the divertor plate is metal, the emitted IR from the surface is low and the surface reflects nearby hot objects. A nearby carbon surface such as the private flux dome at a lower temperature that reflects in the plate may provide more thermal signal than the metal plate at higher temperature. This makes an accurate measurement of the surface temperature of the metal plate difficult or impossible. Reflection of a cold object can also cause confusion.

Reichle et al. have observed non-thermal emission spectra with enhanced emission at shorter wavelengths ascribed to the presence of surface dust of a size smaller than the emission wavelength [9,10] in sub-pixel hot-spots as mentioned above. In ITER, the inclination of the divertor plate will reduce the collection of dust there. Deposited power on the plate will vaporize dust particles, which are poorly coupled to the cooling system. However, dust collected in areas not hit by the steady-state heat flux profile will be rapidly heated by transient events including ELMs and disruptions, indicating a spuriously high surface temperature for a short time.

3.2. Plasma effects

The present ITER design uses carbon at the OSP, nearby tungsten, and beryllium in the main chamber. A thin deposition of metal on the carbon could reduce the emissivity by half or more and cause a large error in the indicated surface temperature. If a deposited layer is low-density and/or poorly adhered to the substrate, transient heating will produce a very rapid temperature increase and fall that is not indicative of damage to the bulk material [11].

If metal is deposited on a carbon surface, the indicated temperature from a single-color system becomes too low. If carbon is deposited on a metal plate, the surface temperature will read too high. A two-color or multi-color IR system would address this. We expect that the OSP will be a region of net erosion, and no deposited layers will remain there. It is likely instead that the OSP will be a source of material for depositing layers elsewhere. The surface layers will mainly affect the measurement of heat deposited by ELMs and disruptions outside the normal strike area.

The small-scale cracking and roughness observed in materials exposed to high heat flux [12] will make the materials more efficient thermal radiators than a new, polished surface. There will likely be significant changes to the divertor plate emissivity during the first diverted ITER discharge. This problem is again best dealt with by using at least a two-color system.

Very high-density cold plasma in the detached regions of the ITER divertor will emit copious radiation from molecular hydrogenic lines at wavelengths less than 3 mm. The wings of the emission line may overlap the wings of the bandpass filter of an IR camera nominally sensitive from 3 to 5 μm, resulting in plasma emission contaminating the thermal signal from the surface. Additional wavelength filtering can reject the molecular emission.

The plasma will emit bremsstralung in the wave band of the IR camera. A calculation of the emission [13,14] from an ITER plasma having a flat density profile at $n_e = 10^{14}$ cm^{-3}, $T_e = 15$ keV [15], and $Z_{\text{eff}} = 1.7$, and path length of 10 m, shows emission of the same magnitude as the thermal emission from the surface at 200 °C. This will bias all the detected temperatures upward unless compensated.

3.3. Other effects

Available space in the port plug limits the size of the optics. The present design fits into a double-walled tube of 360 mm internal diameter. Cooling water is to flow between the walls of the tube. Hot IR optics are undesirable because of emission of background thermal radiation. Cold optics are undesirable, because the cold spots become deposition sites. All the optics will be heated by conduction and by nuclear heating. In addition, the first mirror will be heated by charge exchange flux penetrating the entrance aperture. The mechanical design of the system must pay close attention to cooling of the optics.

Neutron flux will damage lenses and windows. In visible light, the optical materials lose their ability to transmit blue light, due to the formation of color centers that absorb the photons. There is some evidence that this damage affects the transmission of IR light much less than visible light [16].

Using characteristics of currently available IR detectors, we calculated that a surface at 200 °C emits enough IR radiation to provide a signal-to-noise ratio $S/N = 256$ (8 bits) at 86 kHz, using an optical design similar to this one [2]. This is significantly faster than the required 20 ms time resolution. This estimate does not include absorption losses in optics.

For visible emission, we have line-integrated photon radiation rates provided by Kukushkin from his modeling of ITER discharges for D_a, and carbon lines at 514.7, 229.8, and 580.6 nm [17] using the B2.5-EIRENE code [18]. The radiation rate for the carbon line at 465 nm was obtained using the 229.8 nm model result along with the branching ratios from the NIST atomic spectra database [19]. Using read noise, dark current, and quantum efficiency similar to available cameras, we obtained the estimated S/N for various lines at different frame rates, for a chord through a bright region of the divertor. We saw that CIV at 580.6 nm does not provide acceptable S/N (<5 at 50 Hz). The CII line at 514.7 nm provides $S/N = 140$ at 50 Hz. The D_a, gives $S/N = 110$ at 2 kHz; for CIII at 229.8 nm, $S/N = 120$ at 2 kHz; and the CIII at 465 nm provides $S/N = 130$ at 5 kHz.

4. Discussion

We introduced here an optical design for visible/IR imaging of the ITER OSP using six of the upper ports of ITER. It provides

4 mm spatial resolution, which is slightly lower than the 3 mm requirement. However, the containing tube for the optics uses up nearly the entire port tube and does not leave room for other diagnostics in the same port. We see by exploring the various issues above that a two-color or multi-color IR system is desirable. The present design does not include a two-color capability. However, it is a straightforward modification to add a wavelength splitter and pass the image to two cameras instead of one. The increased cost of this must be weighed against the clear benefits.

Acknowledgements

This work was performed under the auspices of the US Department of Energy by Lawrence Livermore National Laboratory under Contract DE-AC52-07NA27344. Work supported by the US ITER Project Office.

References

[1] Funded by the US ITER Office.
[2] C.J. Lasnier, L.G. Seppala, K. Morris, J. Ortiz, et al., Visible and infrared optical design for the ITER upper ports, Lawrence Livermore National Laboratory Report UCRL-TR-228629.
[3] C.J. Lasnier, L.G. Seppala, K. Morris, Modified visible and infrared optical design for the ITER upper ports, Lawrence Livermore National Laboratory Report LLNL-TR-403218.
[4] E. Gauthier et al., in: SOFT Conference Paper, ITER-like wide-angle infrared thermography and visible observation diagnostic using reflective optics, 2006.
[5] Y.S. Touloukian, in: Thermophysical Properties of Matter, Thermal Radiative Properties, vol. 7, IFI/Plenum, New York, 1970.
[6] M. Ulrickson, G.G. Pearson, J. Nucl. Mater. 111&112 (1982) 91.
[7] L.I. Jiang-Gang, L.I. Zhi-Xiu, Plasma Sci. Technol. 2 (2000) 369.
[8] R. Reichle et al., Rev. Sci. Instrum. 75 (2004) 4129.
[9] R. Reichle et al., J. Nucl. Mater. 290–293 (2001) 701.
[10] E. Delchambre et al., J. Nucl. Mater. 337–339 (2005) 1069.
[11] A. Herrmann, W. Junker, et al., Plasma Phys. Control Fus. 37 (1995) 17.
[12] Y. Ueda, T. Funabiki, T. Shimada, et al., J. Nucl. Mater. 337–339 (2005) 1010.
[13] T.C. Hender et al., Nucl. Fusion 47 (2007) S128.
[14] M.A. van Zeeland et al., Nucl. Fusion 48 (2008) 092002.
[15] A.J.H. Donne et al., Nucl. Fusion 47 (2007) S337.
[16] T. Shikama, T. Nishitani, et al., Nucl. Fusion 43 (2003) 517.
[17] A.S. Kukushkin, Private Communication to M.E. Fenstermacher, October 10, 2006.
[18] R. Schneider, D. Reiter, H.P. Zehrfeld, B. Braams, M. Baelmans, et al., J. Nucl. Mater. 196–198 (1992) 810.
[19] Nist.gov, January 2007. <http://www.physics.nist.gov/PhysRefData/ASD/lines_form.html>.